Heparan sulfate deficiency leads to Peters anomaly in mice by disturbing neural crest TGF-β_2 signaling

Keiichiro Iwao,[1,2] Masaru Inatani,[1] Yoshihiro Matsumoto,[3,4] Minako Ogata-Iwao,[1] Yuji Takihara,[1] Fumitoshi Irie,[4] Yu Yamaguchi,[4] Satoshi Okinami,[2] and Hidenobu Tanihara[1]

[1]Department of Ophthalmology and Visual Science, Kumamoto University Graduate School of Medical Sciences, Kumamoto, Japan. [2]Department of Ophthalmology, Faculty of Medicine, Saga University, Saga, Japan. [3]Department of Orthopaedic Surgery, Kyushu University School of Medicine, Fukuoka, Japan. [4]Burnham Institute for Medical Research, La Jolla, California, USA.

During human embryogenesis, neural crest cells migrate to the anterior chamber of the eye and then differentiate into the inner layers of the cornea, the iridocorneal angle, and the anterior portion of the iris. When proper development does not occur, this causes iridocorneal angle dysgenesis and intraocular pressure (IOP) elevation, which ultimately results in developmental glaucoma. Here, we show that heparan sulfate (HS) deficiency in mouse neural crest cells causes anterior chamber dysgenesis, including corneal endothelium defects, corneal stroma hypoplasia, and iridocorneal angle dysgenesis. These dysfunctions are phenotypes of the human developmental glaucoma, Peters anomaly. In the neural crest cells of mice embryos, disruption of the gene encoding exostosin 1 (*Ext1*), which is an indispensable enzyme for HS synthesis, resulted in disturbed TGF-β_2 signaling. This led to reduced phosphorylation of Smad2 and downregulated expression of forkhead box C1 (*Foxc1*) and paired-like homeodomain transcription factor 2 (*Pitx2*), transcription factors that have been identified as the causative genes for developmental glaucoma. Furthermore, impaired interactions between HS and TGF-β_2 induced developmental glaucoma, which was manifested as an IOP elevation caused by iridocorneal angle dysgenesis. These findings suggest that HS is necessary for neural crest cells to form the anterior chamber via TGF-β_2 signaling. Disturbances of HS synthesis might therefore contribute to the pathology of developmental glaucoma.

Introduction

Developmental glaucoma is a congenital blinding disease associated with elevated intraocular pressure (IOP) because of anomalies of the drainage structure for the aqueous humor in the eye. The major drainage structure for aqueous humor consists of the iridocorneal angle, which is the place in which the iris and cornea meet (1, 2). Developmental studies have revealed that the iridocorneal angle originates from the periocular mesenchyme and mainly consists of neural crest cells (3, 4). During ocular morphogenesis, these neural crest cells migrate into the eye to create the anterior chamber, which is a small space within the anterior ocular segment (3, 4). The migrating neural crest cells cover the anterior chamber and differentiate into the iridocorneal angle, the corneal endothelium, and the anterior portion of the iris (5–9). Several of the transcriptional factor genes, such as forkhead box C1 (*Foxc1*), paired-like homeodomain transcription factor 2 (*Pitx2*), and paired box gene 6 (*Pax6*), have been identified as the causative genes for developmental glaucoma, and they have been demonstrated to be responsible for the differentiation of the neural crest cells (10–18). In addition to the iridocorneal angle, developmental glaucoma is also highly associated with anomalies in the neural crest–derived tissues such as the corneal endothelium defect (Peters anomaly; OMIM #604229), iris coloboma (Axenfeld-Rieger syndrome; OMIM #180500, %601499, and #602482), cleft palate, jaw defect, and ear deformity (15, 17, 19). Thus, failed differentiation of the neural crest cells causes anterior chamber dysgenesis, which ultimately results in developmental glaucoma.

Both the orderly migration and differentiation of the neural crest cells are controlled by cues from various cell guidance factors, morphogens, and extracellular matrices. The TGF-β_2 superfamily has been found to be especially associated with mediating the differentiation of the ocular neural crest cells (20–22). The genetic disruption of TGF-β_2 causes anterior chamber dysgenesis (20), with TGF-β_2 signaling regulating the expression of the causative genes for developmental glaucoma, *Foxc1* and *Pitx2* (22). On the other hand, extracellular matrix molecules, such as fibronectin, laminin, peanut agglutinin-binding molecules, and chondroitin sulfate proteoglycans, are thought to affect the behavior of the neural crest cells (23–27). However, despite the influence of these molecules in vitro, it has yet to be determined in vivo whether these extracellular matrices are critical factors for neural crest cell development. The drainage structure has been found to have abundant extracellular matrices (28). Both the accumulation and changes of the component in the human trabecular meshwork are thought to affect the aqueous outflow resistance. Abnormal expression of glycosaminoglycans and their glycoproteins, along with proteoglycans in the trabecular meshwork, have been found in human glaucoma (29–31). Heparan sulfate (HS) is a glycosaminoglycan component of the proteoglycans that is expressed in the

Conflict of interest: The authors have declared that no conflict of interest exists.

Nonstandard abbreviations used: *Ext1*^{flox} mice, transgenic mice carrying the loxP-modified *Ext1* allele; Foxc1, forkhead box C1; HS, heparan sulfate; HSPG, HS proteoglycan; IOP, intraocular pressure; Pitx2, paired-like homeodomain transcription factor 2; *Wnt1-CreExt1*$^{flox/flox}$ mice, the mutant carrying homozygous floxed alleles of *Ext1* and an allele of *Wnt1-Cre*.

Citation for this article: *J. Clin. Invest.* **119**:1997–2008 (2009). doi:10.1172/JCI38519.

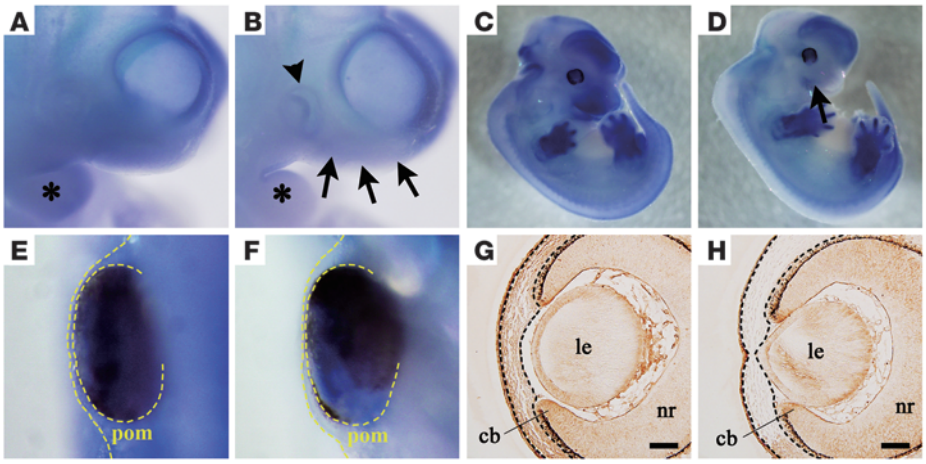

Figure 1
Genetic disruption of *Ext1* and reduced expression of HS in developing neural crest–derived tissues. In situ hybridization for mRNA of *Ext1* at E10.5 (**A** and **B**) and at E12.5 (**C**–**F**). The *Wnt1-CreExt1*$^{flox/flox}$ embryos (**B** and **D**) exhibited weaker signals for *Ext1* mRNA in the head region (black arrows), the branchial arches (asterisks), and the optic vesicle (arrowhead) as compared with the control embryos (**A** and **C**). *Wnt1-CreExt1*$^{flox/flox}$ embryos (**F**) also showed weaker signals in the periocular mesenchyme (yellow dotted lines) as compared with the control embryos (**E**). Immunohistochemistry for HS in ocular tissues at E13.5 (**G** and **H**). While control embryos (**G**) showed broad expression of HS, the *Wnt1-CreExt1*$^{flox/flox}$ embryos (**H**) displayed weak staining for HS in the periocular mesenchymal cells (black dotted lines). cb, ciliary body; le, lens; nr, neural retina; pom, periocular mesenchyme. Scale bar: 50 μm. Original magnification, ×40 (**A** and **B**); ×80 (**E** and **F**).

extracellular matrix of the iridocorneal angle and on cell surfaces of the trabecular meshwork cells (32, 33). Interestingly, genetic studies in *Drosophila* showed that the defect of a HS proteoglycan (HSPG) homolog, *dally*, disturbs signaling mediated by the TGF-β homolog, *dpp,* suggesting that TGF-β–mediated morphogenesis may be dependent upon HSPGs (34). Moreover, a genetic interaction between the HSPG homolog, UNC-52, and the TGF-β homologs is observed during the development of the *Caenorhabditis elegans* gonad arm (35). Therefore, we hypothesized that HS/HSPGs may contribute to the development of the ocular neural crest cells. HS synthesis is governed by a series of enzymes. Exostosin 1 (EXT1) is indispensable for HS synthesis, because it has a critical role in the polymerization process of the alternating D-glucuronic acid and *N*-acetyl-D-glucosamine that ultimately provide the HS sugar chain backbone (36–38). *Ext1*-disrupted cells exhibit a complete loss of HS (37). In the current study, we found that the disruption of *Ext1* in the neural crest cells leads to the Peters anomaly phenotype in the anterior chamber and, thus, affects the TGF-β_2–mediated morphogenesis. We also found that gene reduction of *Ext1* and *Tgfb2* results in developmental glaucoma with an elevated IOP. This suggests that the neural crest cells require HS for TGF-β_2–dependent iridocorneal angle development.

Results

Loss of Ext1 and HS in neural crest–derived tissues of the Wnt1-CreExt1$^{flox/flox}$ *mutant*. *Ext1* mRNA was broadly expressed throughout the embryo. Similar to a previous report, intense signals for *Ext1* were especially observed at E10.5 in the head region and branchial arches of the embryo (Figure 1A) (39). Subsequently, we demonstrated that *Ext1* was particularly localized in the forebrain, hindbrain, facial region, and limb buds at E12.5 (Figure 1C). In order to conditionally disrupt *Ext1* in the neural crest cells during embryogenesis, transgenic mice carrying the loxP-modified *Ext1* allele (*Ext1*^{flox} mice) were bred to transgenic mice with *Cre* recombinase driven by the *Wnt1* promoter (*Wnt1-Cre* mice). The mutant carrying homozygous floxed alleles of *Ext1* and an allele of *Wnt1-Cre* (*Wnt1-CreExt1*$^{flox/flox}$ mice) exhibited substantially decreased signals for *Ext1* mRNA in the branchial arches and the facial region, including the optic vesicle at E10.5 (Figure 1B). In spite of the intense signal of the control (Figure 1, C and E), loss of the signal for the periocular mesenchyme of the mutant occurred at E12.5 (Figure 1, D and F). As compared with the control tissue, immunohistochemistry with an anti-HS antibody revealed there was little staining for the mutant periocular mesenchyme (Figure 1H). The other ocular tissues (including the lens, presumptive ciliary body, and neural retina) in the mutant (Figure 1H) showed similar levels of expression to those in the control (Figure 1G).

HS deficiency causes a Peters-like anomaly. All of the mutants died within the first day of life. Appearance was grossly normal except for severe malformation of the craniofacial tissues such as cleft palate (Figure 2, A–F) and ear deformity (Figure 2, A and B). Eyes of mutants exhibited multiple anomalies. All the eyes of mutants displayed eyelid defects (Figure 2, G–I). Of the 67 mutants at E18.5, 66 (98.5% of the total mutants) had ventral iris coloboma (Figure 2H). The coloboma was consecutively observed in the ciliary body of 39 (58.2%) mutants (Figure 2I). The anterior chamber structure was also affected in the mutant, with an abnormally thin cornea and dysgenesis of the iridocorneal angle (Figure 3, A and B). While a histological study showed that the values of the mutant corneal thickness and anterior chamber depth were significantly smaller than those of the control (Figure 3, A and C), the size of the lens derived from the surface ectoderm was not affected (Figure 3C). Van Gieson staining revealed that collagen was not distributed in the mutant corneal stroma (Figure 3D). Each of the corneal endothelial cells expressed ZO-1, a tight junction protein, in

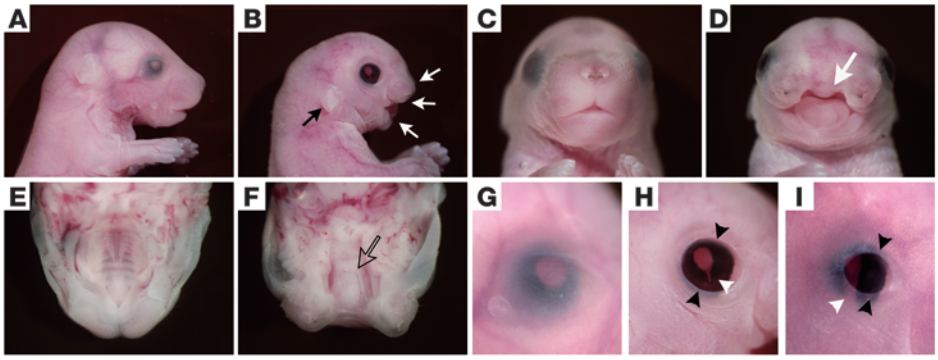

Figure 2
HS deficiency causes craniofacial malformation. Stereomicroscopy for control embryos (**A**, **C**, **E**, and **G**) and *Wnt1-CreExt1*$^{flox/flox}$ embryos (**B**, **D**, **F**, **H**, and **I**) at E18.5. The mutant embryos showed ear deformity (black arrow in **B**), severe cleft palate (white arrows in **B** and **D**), and the lack of a hard palate (open arrow in **F**). The eyes of mutants also displayed eyelid defects (black arrowheads) and iris coloboma (white arrowhead in **H**). Some colobomas affected both the iris and ciliary body (white arrowhead in **I**). Original magnification, ×3.2 (**G**–**I**).

the cell margins (Figure 3E). Immunostaining for ZO-1 revealed loss of ZO-1–positive cells in the mutant corneal endothelium (Figure 3E). These phenotypes in the anterior chambers are very similar to the ocular phenotypes of Peters anomaly, which is associated with disturbed differentiation of the ocular neural crest cells. Moreover, both a histological study performed between E11.5 and E18.5 (Figure 3, A and B) and a fate-mapping study for the neural crest cells (Figure 3F) demonstrated that neural crest cells of the mutant migrated to the periocular mesenchyme as early as E11.5. However, the subsequent developmental steps did not progress to the point in which they formed a distinct anterior chamber.

HS deficiency disturbs neural crest cell proliferation in the anterior chamber. An abnormally thin cornea and hypoplastic iridocorneal angle may be associated with diminished proliferation or enhanced apoptosis of the neural crest cells. In utero BrdU labeling revealed that cell proliferation was decreased in the mutant cornea and iridocorneal angle at E15.5 (Figure 4). However, there were no differences in the frequency of the apoptotic cells observed (data not shown).

To exclude the possibility that decreased numbers of BrdU-positive cells in the mutant corneal stroma were due to limited number of cells in the thinner mutant corneal stroma at E15.5, we counted both the number of BrdU-positive cells and the total corneal cells during the earlier embryonic stage (E13.5). No differences for the corneal thickness or the distribution of neural crest cells (β-gal–positive cells traced by *Rosa26R* mouse strain) were noted between the mutant and control at E13.5. However, there was a significant (Figure 4J) reduction in the number of BrdU-positive cells in the mutant corneal tissue. These results indicated that reduced mutant neural crest cell proliferation is associated with poor anterior chamber development.

HS deficiency is associated with the inactivation of TGF-β_2 signaling and downregulation of Foxc1 and Pitx2. The characteristics of the phenotypes in the anterior chamber were similar to those of the mutant genes for the TGF-β_2 signaling molecules (Figure 5, A and B) (20, 22). Binding assays demonstrated that TGF-β_2 had an affinity to HS, whereas epidermal growth factor did not bind to HS (Figure 5C). If there is disturbance of the TGF-β_2 signaling in the HS-deficient eye, then there should be activation of downstream mediators of TGF-β_2. It has been previously reported that TGF-β_2 expression in the ocular anterior segment peaks between E13.5 and E15.0 (22). In the current study, while no major changes were noted for TGF-β_2 distribution in the mutant eye at E13.5 (Figure 5, D and I), there was specific inhibition, in the periocular mesenchyme of the mutant, of the phosphorylation of Smad2, which is a downstream molecule of TGF-β_2 (Figure 5, E, F, J, and K). Previous studies have demonstrated that *Foxc1* and *Pitx2* encoding transcriptional factors in the neural crest cells are the causative genes for developmental glaucoma (12, 13, 15, 17). The expression of these factors is dependent upon the activation of the TGF-β_2 signaling (22). At E15.5, Pitx2 was observed in the cornea (Figure 5H), and there was localized expression of Foxc1 in the corneal endothelium and primitive trabecular beam (Figure 5G). In the mutant eye, however, a dramatic downregulation of Foxc1 and Pitx2 expression was noted (Figure 5, L and M). This reduced expression of the downstream molecules suggests that the HS deficiency is responsible for the disturbances in the TGF-β_2 signaling.

In addition, it has also been shown that *Tgfb2*-disrupted mutants exhibit cleft palate (40). In the palatal tissue of these HS-deficient embryos, a dramatic downregulation of the immunoreactivity of phosphorylated Smad2 was observed (Supplemental Figure 1; supplemental material available online with this article; doi:10.1172/JCI38519DS1).

FGFs are known to be HS-binding morphogens, which are essential factors for HS-mediated lens development (41). Thus, it is possible that FGF signaling might be involved with anterior chamber morphogenesis. To further study this, we examined the expression of phosphorylated ERK1/2, which are downstream effectors of the FGF-MAPK pathway (Supplemental Figure 1). However, no differences in the phosphorylated ERK1/2 immunoreactivity in the anterior chamber were found between the mutant and control.

TGF-β_2 signaling in neural crest cells requires cell-autonomous expression of HS. The transfection of the adenovirus that encodes the Cre recombinase gene showed there was expression of Cre recombinase in the cultured periocular neural crest cells with the *Ext1*$^{flox/flox}$ alleles (Figure 6A). Immunocytochemistry with the anti-HS antibody showed that the transfection of the Cre recombinase gene caused a loss of HS in the neural crest cells (Figure 6A). In primary cultures of periocular neural crest cells, TGF-β_2–depen-

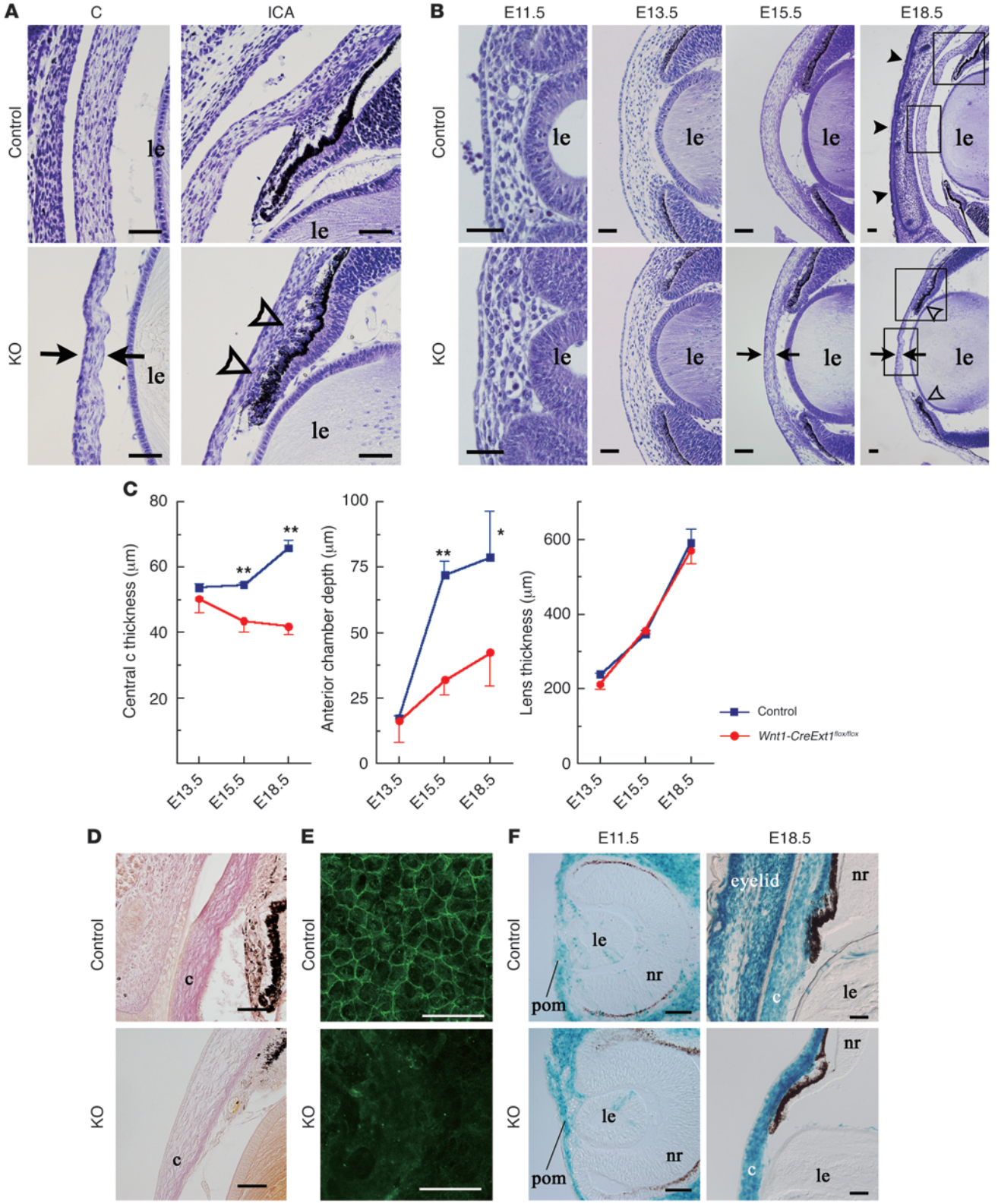
A
C
ICA
Control
KO
le
B
E11.5
E13.5
E15.5
E18.5
C
Central c thickness (μm)
Anterior chamber depth (μm)
Lens thickness (μm)
Control
Wnt1-CreExt1flox/flox
D
E
F
c
pom
nr
eyelid

Figure 3
HS deficiency causes Peters-like anomaly. (**A** and **B**) Thionin staining of the eyes of *Wnt1-CreExt1*$^{flox/flox}$ and control embryos during embryonic development. At E15.5 and E18.5, *Wnt1-CreExt1*$^{flox/flox}$ embryos exhibited abnormal thinning of the central cornea (arrows) and dysgenesis of the iridocorneal angle (open arrowheads). While the control eye shows lid closure (black arrowheads in **B**), the mutant embryo lacked eyelids. Boxed regions in **B** indicate the areas shown at higher magnification in **A**. (**C**) Impaired ocular growth in *Wnt1-CreExt1*$^{flox/flox}$ embryos. The central cornea thickness and the anterior chamber depth in the mutant embryos were significantly smaller, as compared with the control eyes. However, the lens thickness was not affected in the eyes of mutants. (**D**) Van Gieson staining revealed collagen accumulation in the control corneal stroma. In contrast, *Wnt1-CreExt1*$^{flox/flox}$ embryos lacked collagen matrix. (**E**) Immunohistochemistry using anti–ZO-1 antibody exhibited a defect of the endothelial layer in the mutant cornea. (**F**) Fate mapping for neural crest cells. Cre-positive neural crest cells had already migrated to the periocular region as early as E11.5, while the neural crest cells remained distributed at E18.5. Data represent mean ± SEM. $^{*}P < 0.05$, $^{**}P < 0.01$, Student's *t* test ($n = 6$). c, cornea; ICA, iridocorneal angle; KO, *Wnt1-CreExt1*$^{flox/flox}$. Scale bar: 50 μm.

dent BrdU incorporation was observed. However, HS-deficient neural crest cells showed significantly less TGF-β_2–dependent incorporation of BrdU than HS-positive cells did (Figure 6C). In addition, without TGF-β_2–stimulation, these HS-deficient cells were found to have the same level of BrdU-positive cells as did HS-positive cells (Figure 6, B and C). Moreover, immunoblotting that used the anti-Smad2 antibody revealed that the HS-deficient neural crest cells exhibited a loss of activation of Smad2 after TGF-β_2 stimulation (Figure 6D).

The reduction of TGF-β_2–dependent BrdU incorporation in HS-deficient neural crest cells suggested that the HS that is expressed on the cell surface is critical in order for TGF-β_2–induced cell proliferation to occur. To further confirm this hypothesis, HS-deficient neural crest cells were cocultured with HS-positive neural crest cells. The TGF-β_2–induced BrdU incorporation was then analyzed. As shown in Figure 6, E and F, the HS deficiency in the cocultured neural crest cells resulted in a reduced BrdU incorporation after TGF-β_2 stimulation. Thus, these data indicated that TGF-β_2 signaling in neural crest cells requires cell-autonomous expression of HS.

Haploinsufficiency of Ext1 and Tgfb2 causes developmental glaucoma. If TGF-β_2 signaling in the anterior chamber development is dependent upon HS, then the ocular phenotypes of the *Tgfb2* mutants should be enhanced when there is a reduction of 1 allele of *Ext1*. Compound mutants that had a haploinsufficiency of *Ext1* and *Tgfb2* were able to survive and reached adulthood. The eyes of these mutants exhibited a significantly reduced cell number in the trabecular beam and a defect of Schlemm canal, both of which are major components of the aqueous humor drainage structure in the iridocorneal angle (Figure 7, A, D, and E). In contrast, there were no major changes in the iridocorneal angles of the mutants when there was heterozygotic deletion of *Ext1* (Figure 7B) or *Tgfb2* (Figure 7C). Moreover, the compound mutants showed significant IOP elevations (Figure 7F). This was in contrast to each of the heterozygotes, which had IOP levels that were the same as the wild type (Figure 7F). These results indicated that iridocorneal angle development depends on the interaction between HS and TGF-β_2 signaling.

Discussion

In the present study, genetic disruption of *Ext1* in neural crest cells caused anterior chamber dysgenesis, similar to that which is observed in Peters anomaly in humans. In addition, the anterior eye segment exhibited reduced phosphorylation of Smad2 and downregulated expression of Pitx2 and Foxc1, which are the downstream molecules of TGF-β_2. Moreover, in vitro BrdU assays indicated that the TGF-β_2 signaling in neural crest cells was dependent on the HS that is expressed by the cell itself (cell autonomous). When there is a reduced interaction between TGF-β_2 and HS, this can lead to an elevated IOP that is associated with decreased cell numbers in the trabecular beam and the loss of Schlemm canal. Overall, the present study demonstrated that in order for morphogenesis to occur in the anterior chamber of the eye, neural crest cells require an interaction between the TGF-β_2 and HSPGs that are expressed cell autonomously. When there is impaired interaction, this leads to developmental glaucoma.

In humans, the major phenotypes found for Peters anomaly include defects of the corneal endothelium, Descemet membrane, and posterior corneal stroma (42, 43). Patients with Peters anomaly also have a high association with anomalies in other craniofacial neural crest–derived tissues such as ear deformities and cleft palates (19, 44). This association strongly suggests that the pathogenesis of Peters anomaly depends upon the maldevelopment of the craniofacial neural crest cells. In some pedigrees, the inheritance has been described as being autosomal dominant (11) or autosomal recessive (45, 46), while in others it has been stated as being sporadic (47). This suggests that there are multiple causative genes for Peters anomaly. Although large subsets of Peters anomaly cases occur without any molecular characterization, a mutation of *PITX2* is highly associated with Peters anomaly. When there is a loss of *PITX2*, this leads to a defect of the corneal endothelium and corneal stroma, which indicates an essential role for this gene in corneal development (48). PITX2 promotes collagen synthesis via the activation of the protocollagen lysyl hydroxylase (14). In the current study, the HS-deficient mutant manifested ocular phenotypes associated with Peters anomaly, presenting both downregulated expression of Pitx2 and reduced collagen in the corneal stroma. These data provided support for a role for HS in the regulation of the expression of Pitx2 in ocular development that leads to corneal phenotypes. However, in order to regulate the expression of intracellular Pitx2 in the neural crest cells, extracellular HS is required for an interaction with a morphogen, which in this case is the upstream molecule of Pitx2. For anterior chamber development, TGF-β_2 is the most critical morphogen (20). In mammals, there are 3 members of the TGF-β family that are known to exist: TGF-β_1, TGF-β_2, and TGF-β_3 (49, 50). Since TGF-β_2 predominates in the eye during embryonic development, no anomalies are seen in the eyes of either TGF-β_1– or TGF-β_3–null mice (20). However, TGF-β_2–null embryos exhibit Peters ocular phenotypes (20) and cleft palate (40), similar to the phenotype seen for the HS-deficient embryo. Lyon et al. (51) performed affinity chromatography and demonstrated that there are 2 TGF-βs, TGF-β_1 and TGF-β_2, that can bind to heparin and highly sulfated HS. The binding assay in the current study confirmed this affinity between HS and recombinant TGF-β_2. Moreover, HS-deficient neural crest cells in vitro failed to show TGF-β_2–dependent proliferation without the phosphorylation of Smad2, which is a downstream mediator specific to TGF-β.

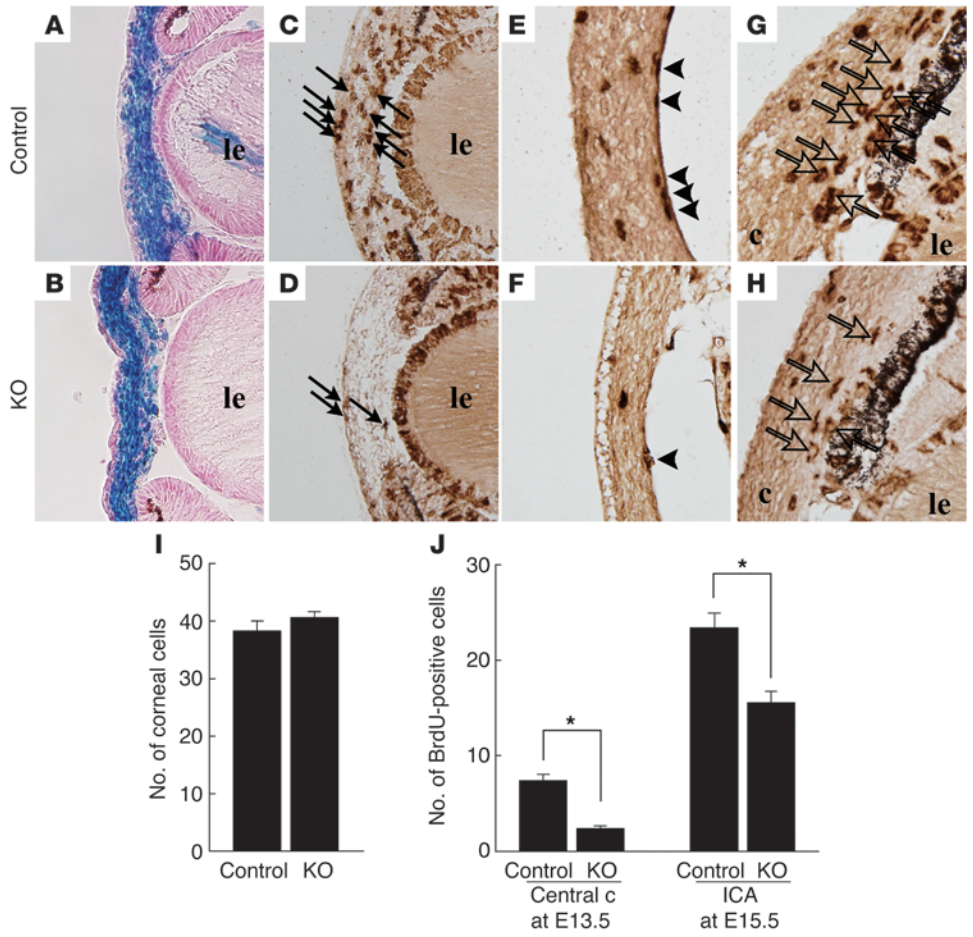

Figure 4

BrdU-labeled neural crest cells in the embryonic anterior ocular segments. At E13.5, there were no differences found for the distribution and the number of β-gal–positive neural crest cells between the *Wnt1-CreExt1*$^{flox/flox}$ embryos (**B** and **I**) and control embryos (**A** and **I**). There was a significantly smaller number of BrdU-labeled cells in the central cornea (arrows) in the stroma of the *Wnt1-CreExt1*$^{flox/flox}$ embryos (**D**) as compared with the control embryos (**C**). Moreover, only a small number of BrdU-labeled cells were present in the corneal endothelium (arrowheads in **E** and **F**) at E15.5. (**G** and **H**). In mutant embryos at E15.5, BrdU-positive cells in the iridocorneal angle (open arrows) were also decreased. Original magnification, ×20 (**A**–**H**). (**J**) The total number of BrdU-positive cells in the central cornea and iridocorneal angle in the mutant embryos was significantly smaller, as compared with the control eyes. Data represent mean ± SEM. *P < 0.01, Student's t test (n = 6).

When taken together, our results indicated that the loss of HS disturbs the TGF-β_2 signaling pathway in the ocular neural crest cells and, thus, leads to the Peters phenotypes.

There are 2 modes of action that HS employs to control the TGF-β_2 signaling. First, HS modulates the diffusion and the gradient of TGF-β_2 within the local environment. For example, the *Drosophila* TGF-β homolog, Dpp, moves along the cell surface via restricted extracellular diffusion that involves HSPGs (52). When there is a loss of HSPGs, this disturbs Dpp-dependent wing disc development. However, in the present study, we found that the distribution of TGF-β_2 was not affected in the mutant periocular mesenchyme, suggesting that there is a smaller contribution of the morphogen gradient for TGF-β_2–induced morphogenesis of the anterior chamber. The second mode of action involves promotion of the interaction between TGF-β_2 and the receptors by the HSPGs on the cell surface. For example, another morphogen, FGF, requires cell-surface HS as a coreceptor for FGF signaling, which combines to form a 2:2:1 ratio that consists of a FGF/FGF receptor/HS ternary complex (53). Our present data strongly suggested that HS on the cell surface of neural crest cells modulates the ligand-receptor interaction for TGF-β_2 (Figure 8).

Because several HS-binding morphogens and growth factors can contribute to the craniofacial development, interactions between morphogens/growth factors other than TGF-β_2 and HS may also be impaired in HS-deficient ocular neural crest cells. Previous studies have reported that genetic disruption of *Fgf8* and *Shh* in the neural crest caused facial dysmorphism (54–56). In addition, the loss of *Fgf8* has been shown to induce defects of the eyelids and outer ears (55). However, these ocular phenotypes are not similar to Peters anomaly. A variety of ocular abnormalities, including the iridocorneal angle hypoplasia and elevated IOP, have been reported in heterozygous *Bmp4* mutants (21). However, reduced corneal stroma or corneal endothelial defects were not found in the *Bmp4* mutant (21). We also did not find any significant disturbance of the phosphorylation of Smad1/5/8 (data not shown) or the phosphorylation of ERK1/2

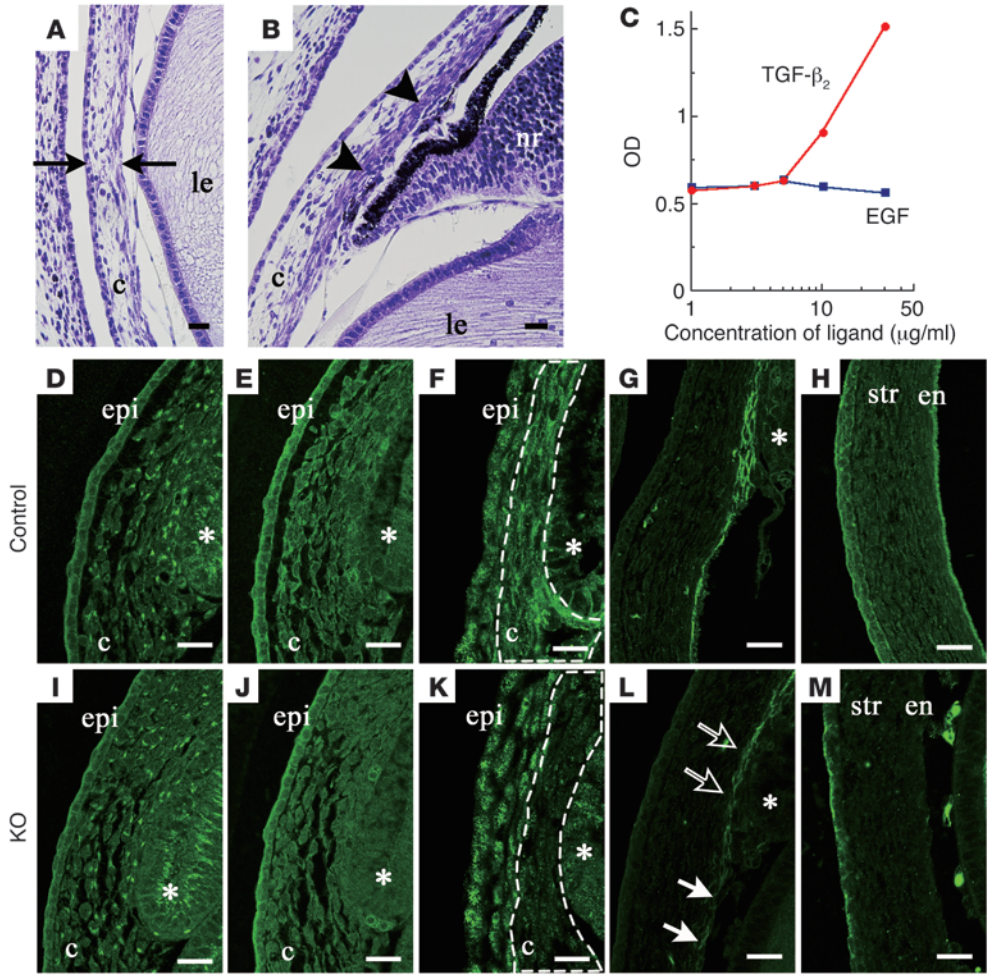

Figure 5

HS deficiency leads to the inactivation of TGF-β_2 signaling and downregulation of the transcription factors Foxc1 and Pitx2. A thin cornea (black arrows in **A**) and iridocorneal dysgenesis (black arrowheads in **B**) were observed in the mutant embryos that lacked the gene for TGF-β_2 (E18.5). (**C**) Binding assay indicated that HS had an affinity for TGF-β_2 but not for EGF. Immunohistochemical staining of TGF-β_2 (**D** and **I**), Smad2 (**E** and **J**), and phosphorylated Smad2 (**F** and **K**) in the iridocorneal angle of the E13.5 embryo, and Foxc1 (**G** and **L**) and Pitx2 (**H** and **M**) in the anterior eye segment of the E15.5 embryo. A disturbance was noted for the phosphorylation of Smad2 in the periocular mesenchyme (dotted lines in **F** and **K**) in the *Wnt1-CreExt1*$^{flox/flox}$ embryos. In the eyes of mutants, the expression of Foxc1 was substantially reduced in the corneal endothelial layer (white arrows) and in the iridocorneal angle (open arrows), while Pitx2 expression was hardly detected in the corneal stroma or endothelium. en, corneal endothelium; epi, corneal epithelium; str, corneal stroma; *, presumptive ciliary body. Scale bar: 20 μm.

(Supplemental Figure 1), which are downstream mediators of BMP4 (57) and FGFs, respectively, in the HS-deficient anterior ocular segment. Taken together, even though we were not able to completely exclude the possibility that other HS-binding morphogens were affected in the HS-deficient anterior chamber, the phenotypical similarities strongly suggested there is a predominant role for HS in the TGF-β_2–dependent development of ocular neural crest cells.

In the compound mutant, haploinsufficiency of *Ext1* and *Tgfb2* causes hypoplasia of the iridocorneal angle, resulting in IOP elevation. Phenotypes of the compound mutant mice suggest that an impaired TGF-β_2–HS interaction leads to developmental glaucoma. Recent reports have indicated that TGF-β_2 is involved in the pathogenesis of primary open-angle glaucoma (POAG) (58). It has also been reported that there are elevated concentrations of TGF-β_2 in the aqueous humor of eyes with POAG (59–61) and in developmental glaucoma (61). The trabecular tissue in developmental glaucoma is associated with an abnormal distribution of HS that exhibits an abnormal accumulation (29) or a significant loss (31). These findings may indicate that improper expression of TGF-β_2 and HS can promote the immaturity of the anterior chamber angle in developmental glaucoma or cause impaired cellular function in the trabecular meshwork and Schlemm canal of POAG. To determine the role of HS in human developmental glaucoma, further genomic analyses designed to examine the HS-synthesizing enzymes in patients with developmental glaucoma are required.

In conclusion, we have demonstrated that HS is an essential factor required for proper differentiation and proliferation of the ocular neural crest cells in the anterior chamber. When there

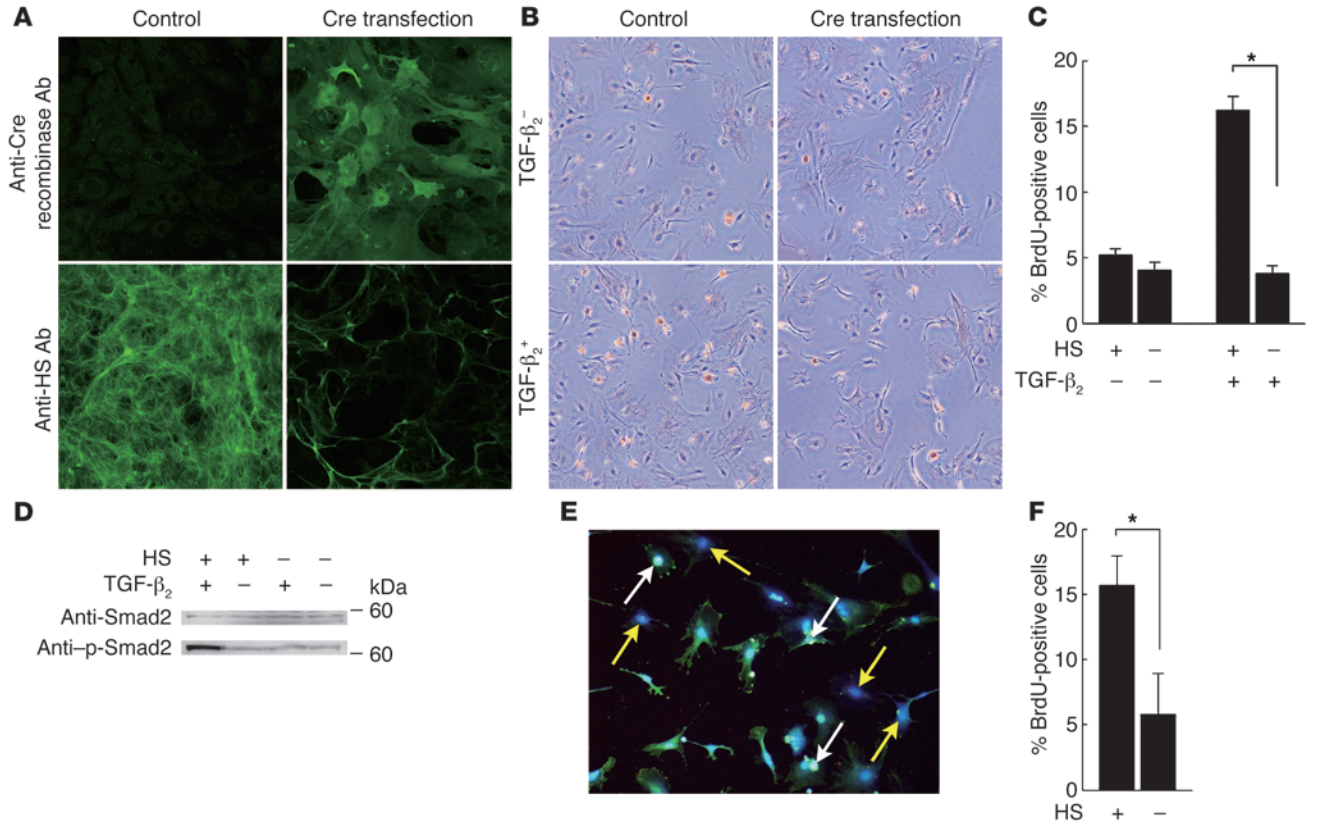

Figure 6

Disturbed TGF-β_2–stimulated proliferation of HS-deficient neural crest cells. (**A**) Immunostaining with anti-HS and anti-Cre recombinase antibodies indicated that there were Cre-transfected periocular neural crest cells with *Ext1*$^{flox/flox}$ alleles that expressed Cre recombinase while having lost HS. (**B** and **C**) BrdU proliferation assay. While the periocular neural crest cells showed TGF-β_2–dependent BrdU incorporation (orange-colored cells), the HS-deficient neural crest cells had a low rate of BrdU-positive cells. There was a statistical significance found for the TGF-β_2–dependent proliferation between the HS-positive and HS-deficient cells. (**D**) Western blot for Smad2 and phosphorylated Smad2 (p-Smad2) was analyzed in the cultured cells. While TGF-β_2 enhanced the phosphorylation of Smad2, there was no phosphorylation of Smad2 in the HS-deficient neural crest cells, even after TGF-β_2 stimulation. (**E** and **F**) BrdU proliferation assay in cocultures of HS-positive and HS-deficient cells. Since the HS, BrdU, and nucleus were labeled by FITC (green), Alexa Fluor 568 (red), and Hoechst 33258 (blue), respectively, the BrdU-positive cells exhibit a white-colored nucleus (white arrows) in HS-positive cells, while they have a magenta-colored nucleus in HS-deficient cells. A significant reduction of the BrdU-positive cells was seen in the HS-deficient cells (yellow arrows). (**F**) The comparison of the percentage of BrdU-positive cells between HS-positive and HS-negative cells in coculture. Data represent mean ± SEM. *$P < 0.01$, Student's t test ($n = 9$). Original magnification, ×10 (**A**, **B**, and **E**).

is HS deficiency, this leads to severe anterior chamber dysgenesis, which is reminiscent of Peters anomaly in humans. In addition, the impaired interaction between TGF-β_2 and HS causes developmental glaucoma. These findings suggest that disturbances in the synthesis of HS might contribute to the pathology of developmental glaucoma.

Methods

Mice. The mutant mouse strains used in this study have all been reported previously (6, 22, 39, 62). To produce mutant mice with the *Ext1*-deficient periocular mesenchymal cells during embryogenesis, *Wnt1* promoter-driven *Cre*-transgenic mice (The Jackson Laboratory) were mated with mice carrying the *Ext1*^{flox} allele. Subsequently, in order to obtain mutants with a *Wnt1-CreExt1*$^{flox/flox}$ genotype, the *Wnt1-CreExt1*$^{flox/wild}$ male mice were crossed with female mice that were homozygous for the *Ext1*^{flox} allele. Littermates carrying *Ext1*$^{flox/flox}$ or *Ext1*$^{flox/wild}$ were used as controls. To detect the neural crest cells in the anterior eye segment, *Wnt1-Cre* transgenic mice were crossed with *Rosa26R* mice (a gift from H. Okita, National Research Institute for Child Health and Development, Tokyo, Japan, and P. Soriano, Mount Sinai School of Medicine, New York, New York, USA) (B6.129-*Gt(ROSA)26Sor*, The Jackson Laboratory), as they express β-gal following Cre-mediated recombination (63). *Tgfb2* transgenic mice (The Jackson Laboratory) were generated via gene targeting, as has been previously reported (40). *Tgfb2* heterozygous mice were mated with *Ext1* heterozygous mice. Genotyping of the mice was performed by PCR-based methods that used DNA prepared from tail biopsies. All of the mice strains used in this study were backcrossed with C57BL/6 more than 10 times. All of the procedures involving the mice were performed in accordance with the *Association for Research in Vision and Ophthalmology Statement for the Use of Animals in Ophthalmic and Vision Research* and the guidelines were approved by the Kumamoto University Committee on the Use and Care of Animals.

Whole-mount in situ hybridization. To study the expression pattern of *Ext1* mRNA in developing embryos, in situ hybridization with a digoxigenin-conjugated riboprobe for *Ext1* was performed, as has been previously reported (39). Briefly, the riboprobe was hybridized at 55°C overnight, fol-

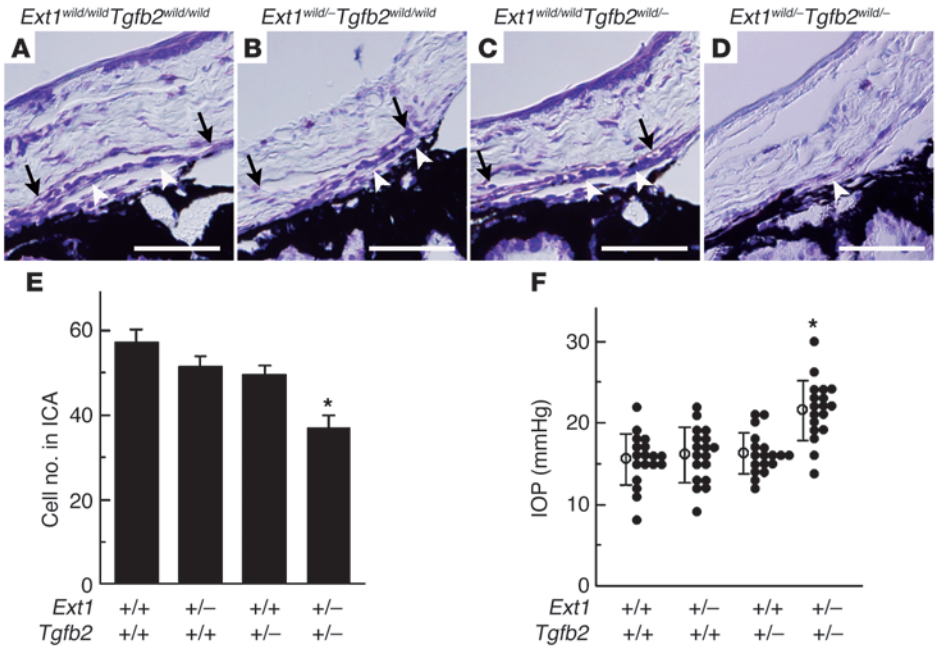

Figure 7
Haploinsufficiency of *Ext1* and *Tgfb2* leads to aberrant iridocorneal development. (**A**) There were no major anomalies noted in Schlemm canal (black arrows) or the trabecular beam (white arrowheads) for either the controls (**A**) or the *Ext1* (**B**) or *Tgfb2* (**C**) haploinsufficient mutants. As compared with the wild-type mice, the double heterozygote mice (**D**) had a hypoplastic trabecular beam, and they lacked a Schlemm canal. The double heterozygote mice also exhibited a significant reduction of the total cell number for the iridocorneal angle (**E**), in addition to an elevated IOP (**F**). Data represent mean ± SEM. $^*P < 0.01$, Student's *t* test ($n = 9$). Scale bar: 50 μm.

lowed by stringent washes. The embryos were then treated with an alkaline phosphatase-conjugated antidigoxigenin antibody (Roche). Hybridization signals were visualized with BM purple AP substrate (Roche).

Histology. Embryos were fixed with Carnoy's fixative solution (6 parts EtOH [absolute or 99.5%], 3 parts chloroform, and 1 part glacial acetic acid) at 4°C for 3 hours, embedded in paraffin, and processed for histological examination. After preparing 4-μm-thick sections, samples were stained with thionin and then histologically examined by light microscopy. Photographs were taken with a DP50 digital camera (Olympus). Samples were stained with van Gieson solution to determine the accumulation of collagen in the cornea. To analyze the ocular size, the thickness of the central cornea and the axial length of the anterior chamber and lens were measured in 5 *Wnt1-CreExt1*$^{flox/flox}$ and 5 control embryos. For analysis of the iridocorneal angle of the *Tgfb2* and *Ext1* double-mutant mice, 6-week-old mice were sacrificed and used to prepare 4-μm-thick paraffin sections. Cell nuclei in the trabecular beam area were counted within a 200-μm-width sampling window, located within the iridocorneal angle. A total of 9 mice were analyzed for each genotype strain.

Immunohistochemistry. Four-micrometer-thick sections fixed with Carnoy's solution or frozen 15-μm-thick sections fixed with 4% paraformaldehyde solution were incubated with primary antibodies. Anti–TGF-β_2 (Lab Vision), anti-Smad2 (Santa Cruz Biotechnology Inc.), anti-phosphorylated Smad2 (Chemicon), anti-phosphorylated ERK1/2 (Cell Signaling Technology), anti-Pitx2 (Santa Cruz Biotechnology Inc.), anti-Foxc1 (Santa Cruz Biotechnology Inc.), and anti-HS, HepSS1 (Seikagaku Corp.) were used as the primary antibodies. For the anti-HS analysis, we used biotin-conjugated anti-mouse IgM as the secondary antibody, the Vectastain Elite ABC kit (Vector Laboratories), diaminobenzidine substrate (Vector Laboratories), and the Entellan New mounting solution (Merck). Fluorescence immunohistochemistry was performed using fluorescein anti-mouse IgM (Vector Laboratories), Alexa Fluor anti-rabbit IgG, and Alexa Fluor anti-goat IgG polyclonal (Molecular Probes Inc.) antibodies as the secondary antibodies. After mounting using ProLong Gold Antifade Reagent (Molecular Probes), the sections were examined using confocal laser microscopy (FV300 and FV500-IX; Olympus).

Fate mapping of the neural crest cells. To analyze the distribution of the neural crest cells in the anterior eye segment, we used the *Rosa26R* mouse strain B6.129-*Gt(ROSA)26Sor* (The Jackson Laboratory), as it expresses β-gal following Cre-mediated recombination (63). Female *Ext1*$^{flox/flox}$*Rosa26R* mice were crossed with male *Wnt1-CreExt1*$^{flox/wild}$ mice to produce mutants with *Wnt1-CreExt1*$^{flox/flox}$*Rosa26R*. The mutant and control mice with *Rosa26R* were stained with X-gal (Sigma-Aldrich). Samples were also counterstained by Contrast RED solution (KPL) for cell counting. We subsequently prepared frozen sections for the analyses.

BrdU labeling of the embryos and TUNEL staining. Timed pregnant female mice (E13.5 and E15.5) were injected intraperitoneally with 200 μg/g body weight of BrdU and then sacrificed 1 hour later. Embryos were removed, fixed in Carnoy's solution at 4°C for 3 hours, and then embedded in paraffin. Samples were cut into 4-μm horizontal sections and stained with anti-BrdU antibody (Chemicon). Samples then underwent sequential incubation with biotin-conjugated anti-mouse IgG antibody, followed by examination using a Vectastain Elite ABC kit (Vector Laboratories) and diaminobenzidine substrate (Vector Laboratories). The numbers of BrdU-positive cells were counted within two 100-μm-width sampling windows (per section), located in the center of the corneal stroma and on both side of the iridocorneal angle. The analyses were conducted in 5 *Wnt1-CreExt1*$^{flox/flox}$ and 5 control embryos. TUNEL assays were performed using the Dead-End Fluorometric TUNEL system (Promega). The 4-μm sections from the embryos at E15.5 were treated with 0.85% NaCl solution and 20 μg/ml proteinase K solution after deparaffinization. After equilibrating, fluorescein-

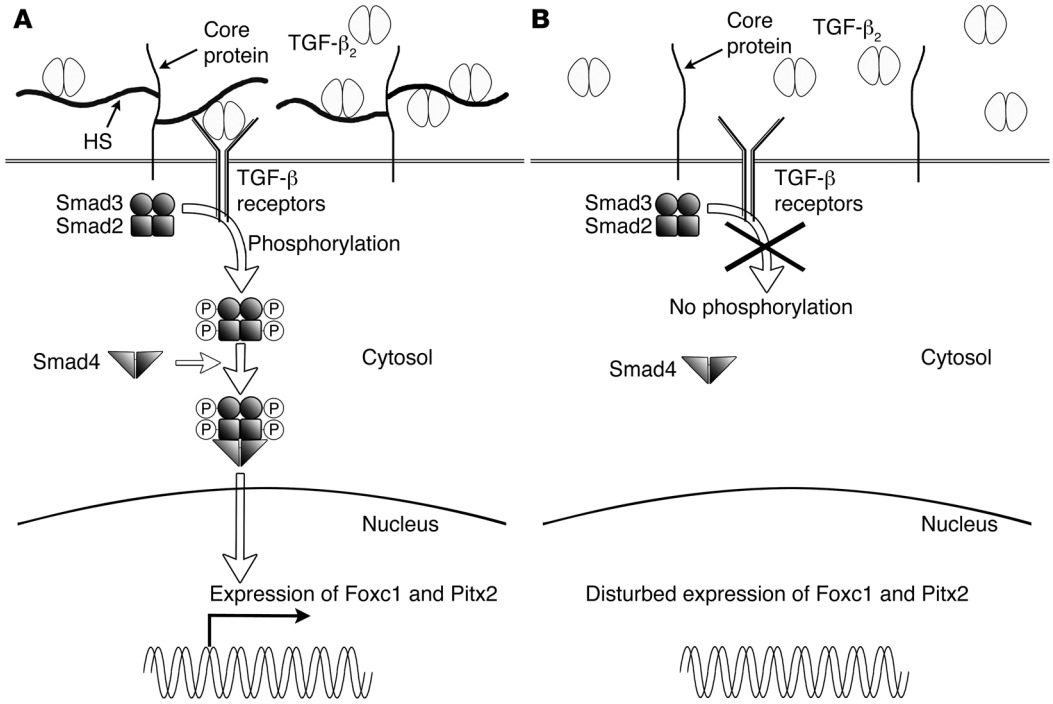

Figure 8
Hypothetical schema of the HS-dependent TGF-β_2 signaling on the cell surface of neural crest cells. (**A**) HS has an affinity for TGF-β_2, which enhances the ligand presentation to the TGF-β receptors. Subsequently, transduction of the signal to the nucleus occurs via phosphorylation of the Smads. (**B**) For the HS defect, there is deterioration of the efficiency of the interaction between TGF-β_2 and the receptors, which leads to a disturbance of the Smads phosphorylation. The loss of phosphorylated Smads then inhibits the expression of Foxc1 and Pitx2.

12–dUTP was then incorporated at the 3′-OH DNA ends through the use of terminal deoxynucleotidyl transferase recombinant enzyme. Sections were then analyzed by confocal laser microscopy (Olympus).

Binding assay. To study the affinity of morphogens for HS, we performed a binding assay that used the ELISA method, as has been previously reported (64). Briefly, TGF-β_2 and epidermal growth factor (R&D Systems) were applied to the polystyrene ELISA tray and incubated for 1 hour at 37°C. After blocking with BSA/PBS, biotinylated HS (Celsus) was then applied to the wells and incubated for 1 hour at 37°C. The bound HS was detected by HRP-conjugated streptavidin and the ELISA kit (BioSource, Invitrogen). The absorbance after the reaction was measured using a Model 550 plate reader (Bio-Rad).

Cell culture and transfection. Periocular mesenchymal tissues were removed from *Ext1*$^{flox/flox}$ embryos at E11.5 by microdissection. The mesenchymal cells were cultured in DMEM/F12 medium (Gibco, Invitrogen) containing 10% fetal bovine serum (Sigma-Aldrich) at 37°C in 5% CO_2. To disrupt the HS synthesis, an adenovirus, which included the sequence (65) of the Cre recombinase that was generated from the cosmid, pAxCANCreit2/*Pac* I (Nippon Gene) was added to cultured periocular mesenchymal cells. The virus solution (2.3×10^9 PFU/ml) was diluted accordingly and then added to the cultured cells for 1 hour at 37°C. For the coculture study, transfected cells were additionally cultured with HS-positive periocular mesenchymal cells for an additional day. After virus transfection, the cells were cultured in DMEM/F12 with 10% fetal bovine serum for 16 hours. To detect the expressions of HS and Cre recombinase, we performed immunohistochemistry using anti-HS and anti-Cre recombinase antibody.

Protein extraction and Western blot analysis. Following a 16-hour incubation in DMEM/F12 containing 0.1% BSA at 37°C, cells were treated with 5 ng/ml of TGF-β_2 (R&D Systems) for 90 minutes at 37°C, as has been previously described (22). Proteins were extracted from cells with RIPA buffer (Thermo Fisher Scientific) that contained protease and phosphatase inhibitor cocktails (Thermo Fisher Scientific). Proteins in the cell extracts were separated by SDS-PAGE and electrotransferred to nitrocellulose membranes (Whatman) at 30 V for 60 minutes using the XCell SureLock Mini-Cell (Invitrogen). The membranes were blocked with 5% normal rabbit serum/Tris-buffered saline containing 0.1% Tween20 (TBST) and 5% skim milk/TBST for the anti-Smad2 (Santa Cruz Biotechnology Inc.) and the anti-phosphorylated Smad2 (Chemicon) antibody reactions, respectively. After the primary antibody reaction, target proteins were detected with HRP-conjugated anti-goat IgG (Jackson ImmunoResearch Laboratories Inc.) and anti-rabbit IgG (Amersham Biosciences) antibodies. Immunopositive bands were visualized by chemiluminescence with the ECL Western Blotting Detection Reagents (Amersham Biosciences) and LAS 4000 Mini UV (Fujifilm).

BrdU proliferation assay in vitro. Following 16 hours of incubation in DMEM/F12 containing 0.1% BSA at 37°C, cells were incubated in DMEM/F12 containing 0.1% BSA and BrdU (final concentration of 10 μM) with or without TGF-β_2 (5 ng/ml) for 12 hours at 37°C. Cells incorporating BrdU were identified by staining with anti-BrdU monoclonal antibody (Chemicon) and 3,3′-diaminobenzidine. After analysis of each of the 9 samples, a Student's *t* test was used to determine the statistical significance.

IOP measurement. IOP was measured using the TonoLab rebound tonometer for rodents (M.E. Technica), according to the manufacturer's recommended procedures. After a few minutes of acclimation, IOPs of conscious mice at P42 were measured between 11:30 AM and 12:30 PM. Statistical significance was determined by Student's *t* test.

Statistics. For statistical comparison of 2 samples, we used a 2-tailed Student's *t* test. *P* values of less than 0.05 were regarded as statistically significant.

Acknowledgments

We thank H. Okita and P. Soriano for their gift of the *Rosa26R* mice and Y. Fukuchi, E. Otsubo, and C. Naito for their experimental assistance. This work was supported in part by Grants-in-Aid for Scientific Research (KAKENHI) (S) 19679008 from the Ministry of Education, Culture, Sports, Science and Technology, Japan (to M. Inatani) and NIH grants R01 NS49641 and P01 HD25938 (to Y. Yamaguchi).

Received for publication January 9, 2009, and accepted in revised form April 22, 2009.

Address correspondence to: Masaru Inatani, Department of Ophthalmology and Visual Science, Kumamoto University Graduate School of Medical Sciences, 1-1-1, Honjo, 860-8556 Kumamoto, Japan. Phone: 81-96-373-5247; Fax: 81-96-373-5249; E-mail: inatani@kumamoto-u.ac.jp.

1. Maul, E., Strozzi, L., Munoz, C., and Reyes, C. 1980. The outflow pathway in congenital glaucoma. *Am. J. Ophthalmol.* **89**:667–673.
2. Tawara, A., and Inomata, H. 1981. Developmental immaturity of the trabecular meshwork in congenital glaucoma. *Am. J. Ophthalmol.* **92**:508–525.
3. Serbedzija, G.N., Bronner-Fraser, M., and Fraser, S.E. 1992. Vital dye analysis of cranial neural crest cell migration in the mouse embryo. *Development.* **116**:297–307.
4. Langenberg, T., Kahana, A., Wszalek, J.A., and Halloran, M.C. 2008. The eye organizes neural crest cell migration. *Dev. Dyn.* **237**:1645–1652.
5. Cvekl, A., and Tamm, E.R. 2004. Anterior eye development and ocular mesenchyme: new insights from mouse models and human diseases. *Bioessays.* **26**:374–386.
6. Gage, P.J., Rhoades, W., Prucka, S.K., and Hjalt, T. 2005. Fate maps of neural crest and mesoderm in the mammalian eye. *Invest. Ophthalmol. Vis. Sci.* **46**:4200–4208.
7. Creuzet, S., Vincent, C., and Couly, G. 2005. Neural crest derivatives in ocular and periocular structures. *Int. J. Dev. Biol.* **49**:161–171.
8. Adler, R., and Canto-Soler, M.V. 2007. Molecular mechanisms of optic vesicle development: complexities, ambiguities and controversies. *Dev. Biol.* **305**:1–13.
9. Iwao, K., Inatani, M., Okinami, S., and Tanihara, H. 2008. Fate mapping of neural crest cells during eye development using a protein 0 promoter-driven transgenic technique. *Graefes Arch. Clin. Exp. Ophthalmol.* **246**:1117–1122.
10. Ton, C.C., et al. 1991. Positional cloning and characterization of a paired box- and homeobox-containing gene from the aniridia region. *Cell.* **67**:1059–1074.
11. Hanson, I.M., et al. 1994. Mutations at the PAX6 locus are found in heterogeneous anterior segment malformations including Peters' anomaly. *Nat. Genet.* **6**:168–173.
12. Semina, E.V., et al. 1996. Cloning and characterization of a novel bicoid-related homeobox transcription factor gene, RIEG, involved in Rieger syndrome. *Nat. Genet.* **14**:392–399.
13. Nishimura, D.Y., et al. 1998. The forkhead transcription factor gene FKHL7 is responsible for glaucoma phenotypes which map to 6p25. *Nat. Genet.* **19**:140–147.
14. Hjalt, T.A., Amendt, B.A., and Murray, J.C. 2001. PITX2 regulates procollagen lysyl hydroxylase (PLOD) gene expression: implications for the pathology of Rieger syndrome. *J. Cell Biol.* **152**:545–552.
15. Honkanen, R.A., et al. 2003. A family with Axenfeld-Rieger syndrome and Peters Anomaly caused by a point mutation (Phe112Ser) in the FOXC1 gene. *Am. J. Ophthalmol.* **135**:368–375.
16. Tamimi, Y., et al. 2006. FGF19 is a target for FOXC1 regulation in ciliary body-derived cells. *Hum. Mol. Genet.* **15**:3229–3240.
17. Strungaru, M.H., Dinu, I., and Walter, M.A. 2007. Genotype-phenotype correlations in Axenfeld-Rieger malformation and glaucoma patients with FOXC1 and PITX2 mutations. *Invest. Ophthalmol. Vis. Sci.* **48**:228–237.
18. Weng, J., et al. 2008. Deletion of G protein-coupled receptor 48 leads to ocular anterior segment dysgenesis (ASD) through down-regulation of Pitx2. *Proc. Natl. Acad. Sci. U S A.* **105**:6081–6086.
19. Traboulsi, E.I., and Maumenee, I.H. 1992. Peters' anomaly and associated congenital malformations. *Arch. Ophthalmol.* **110**:1739–1742.
20. Saika, S., et al. 2001. TGFbeta2 in corneal morphogenesis during mouse embryonic development. *Dev. Biol.* **240**:419–432.
21. Chang, B., et al. 2001. Haploinsufficient Bmp4 ocular phenotypes include anterior segment dysgenesis with elevated intraocular pressure. *BMC Genet.* **2**:18.
22. Ittner, L.M., et al. 2005. Compound developmental eye disorders following inactivation of TGFbeta signaling in neural-crest stem cells. *J. Biol.* **4**:11.
23. Newgreen, D., and Thiery, J.P. 1980. Fibronectin in early avian embryos: synthesis and distribution along the migration pathways of neural crest cells. *Cell Tissue Res.* **211**:269–291.
24. Rovasio, R.A., Delouvee, A., Yamada, K.M., Timpl, R., and Thiery, J.P. 1983. Neural crest cell migration: requirements for exogenous fibronectin and high cell density. *J. Cell Biol.* **96**:462–473.
25. Oakley, R.A., and Tosney, K.W. 1991. Peanut agglutinin and chondroitin-6-sulfate are molecular markers for tissues that act as barriers to axon advance in the avian embryo. *Dev. Biol.* **147**:187–206.
26. Oakley, R.A., Lasky, C.J., Erickson, C.A., and Tosney, K.W. 1994. Glycoconjugates mark a transient barrier to neural crest migration in the chicken embryo. *Development.* **120**:103–114.
27. Dutt, S., Kleber, M., Matasci, M., Sommer, L., and Zimmermann, D.R. 2006. Versican V0 and V1 guide migratory neural crest cells. *J. Biol. Chem.* **281**:12123–12131.
28. Acott, T.S., and Kelley, M.J. 2008. Extracellular matrix in the trabecular meshwork. *Exp. Eye Res.* **86**:543–561.
29. Tawara, A., and Inomata, H. 1994. Distribution and characterization of sulfated proteoglycans in the trabecular tissue of goniodysgenetic glaucoma. *Am. J. Ophthalmol.* **117**:741–755.
30. Knepper, P.A., Goossens, W., Hvizd, M., and Palmberg, P.F. 1996. Glycosaminoglycans of the human trabecular meshwork in primary open-angle glaucoma. *Invest. Ophthalmol. Vis. Sci.* **37**:1360–1367.
31. Kuleshova, O.N., Zaidman, A.M., and Korel, A.V. 2007. Glycosaminoglycans of the trabecular meshwork of the eye in primary juvenile glaucoma. *Bull. Exp. Biol. Med.* **143**:381–384.
32. Rohen, J.W., Schachtschabel, D.O., and Berghoff, K. 1984. Histoautoradiographic and biochemical studies on human and monkey trabecular meshwork and ciliary body in short-term explant culture. *Graefes Arch. Clin. Exp. Ophthalmol.* **221**:199–206.
33. Tawara, A., Varner, H.H., and Hollyfield, J.G. 1989. Distribution and characterization of sulfated proteoglycans in the human trabecular tissue. *Invest. Ophthalmol. Vis. Sci.* **30**:2215–2231.
34. Jackson, S.M., et al. 1997. dally, a Drosophila glypican, controls cellular responses to the TGF-beta-related morphogen, Dpp. *Development.* **124**:4113–4120.
35. Merz, D.C., Alves, G., Kawano, T., Zheng, H., and Culotti, J.G. 2003. UNC-52/perlecan affects gonadal leader cell migrations in C. elegans hermaphrodites through alterations in growth factor signaling. *Dev. Biol.* **256**:173–186.
36. McCormick, C., et al. 1998. The putative tumour suppressor EXT1 alters the expression of cell-surface heparan sulfate. *Nat. Genet.* **19**:158–161.
37. Lin, X., et al. 2000. Disruption of gastrulation and heparan sulfate biosynthesis in EXT1-deficient mice. *Dev. Biol.* **224**:299–311.
38. Lind, T., Tufaro, F., McCormick, C., Lindahl, U., and Lidholt, K. 1998. The putative tumor suppressors EXT1 and EXT2 are glycosyltransferases required for the biosynthesis of heparan sulfate. *J. Biol. Chem.* **273**:26265–26268.
39. Inatani, M., et al. 2003. Mammalian brain morphogenesis and midline axon guidance require heparan sulfate. *Science.* **302**:1044–1046.
40. Sanford, L.P., et al. 1997. TGFbeta2 knockout mice have multiple developmental defects that are non-overlapping with other TGFbeta knockout phenotypes. *Development.* **124**:2659–2670.
41. Pan, Y., Woodbury, A., Esko, J.D., Grobe, K., and Zhang, X. 2006. Heparan sulfate biosynthetic gene Ndst1 is required for FGF signaling in early lens development. *Development.* **133**:4933–4944.
42. Nakanishi, I., and Brown, S.I. 1971. The histopathology and ultrastructure of congenital, central corneal opacity (Peters' anomaly). *Am. J. Ophthalmol.* **72**:801–812.
43. Stone, D.L., Kenyon, K.R., Green, W.R., and Ryan, S.J. 1976. Congenital central corneal leukoma (Peters' anomaly). *Am. J. Ophthalmol.* **81**:173–193.
44. Maillette de Buy Wenniger-Prick, L.J., and Hennekam, R.C. 2002. The Peters' plus syndrome: a review. *Ann. Genet.* **45**:97–103.
45. Frydman, M., Weinstock, A.L., Cohen, H.A., Savir, H., and Varsano, I. 1991. Autosomal recessive Peters anomaly, typical facial appearance, failure to thrive, hydrocephalus, and other anomalies: further delineation of the Krause-Kivlin syndrome. *Am. J. Med. Genet.* **40**:34–40.
46. Hennekam, R.C., et al. 1993. The Peters'-Plus syndrome: description of 16 patients and review of the literature. *Clin. Dysmorphol.* **2**:283–300.
47. Waring, G.O., 3rd, Rodrigues, M.M., and Laibson, P.R. 1975. Anterior chamber cleavage syndrome. A stepladder classification. *Surv. Ophthalmol.* **20**:3–27.
48. Lu, M.F., Pressman, C., Dyer, R., Johnson, R.L., and Martin, J.F. 1999. Function of Rieger syndrome gene in left-right asymmetry and craniofacial development. *Nature.* **401**:276–278.
49. ten Dijke, P., Hansen, P., Iwata, K.K., Pieler, C., and Foulkes, J.G. 1988. Identification of another member of the transforming growth factor type beta gene family. *Proc. Natl. Acad. Sci. U. S. A.* **85**:4715–4719.
50. Derynck, R., et al. 1988. A new type of transforming growth factor-beta, TGF-beta 3. *EMBO J.* **7**:3737–3743.
51. Lyon, M., Rushton, G., and Gallagher, J.T. 1997. The interaction of the transforming growth factor-betas with heparin/heparan sulfate is isoform-specific. *J. Biol. Chem.* **272**:18000–18006.
52. Belenkaya, T.Y., et al. 2004. Drosophila Dpp morphogen movement is independent of dynamin-mediated endocytosis but regulated by the glypican

members of heparan sulfate proteoglycans. *Cell.* **119**:231–244.
53. Pellegrini, L., Burke, D.F., von Delft, F., Mulloy, B., and Blundell, T.L. 2000. Crystal structure of fibroblast growth factor receptor ectodomain bound to ligand and heparin. *Nature.* **407**:1029–1034.
54. Trumpp, A., Depew, M.J., Rubenstein, J.L., Bishop, J.M., and Martin, G.R. 1999. Cre-mediated gene inactivation demonstrates that FGF8 is required for cell survival and patterning of the first branchial arch. *Genes Dev.* **13**:3136–3148.
55. Kawauchi, S., et al. 2005. Fgf8 expression defines a morphogenetic center required for olfactory neurogenesis and nasal cavity development in the mouse. *Development.* **132**:5211–5223.
56. Jeong, J., Mao, J., Tenzen, T., Kottmann, A.H., and McMahon, A.P. 2004. Hedgehog signaling in the neural crest cells regulates the patterning and growth of facial primordia. *Genes Dev.* **18**:937–951.
57. Massague, J., and Chen, Y.G. 2000. Controlling TGF-beta signaling. *Genes Dev.* **14**:627–644.
58. Lutjen-Drecoll, E. 2005. Morphological changes in glaucomatous eyes and the role of TGFbeta2 for the pathogenesis of the disease. *Exp. Eye Res.* **81**:1–4.
59. Tripathi, R.C., Li, J., Chan, W.F., and Tripathi, B.J. 1994. Aqueous humor in glaucomatous eyes contains an increased level of TGF-beta 2. *Exp. Eye Res.* **59**:723–727.
60. Inatani, M., et al. 2001. Transforming growth factor-beta 2 levels in aqueous humor of glaucomatous eyes. *Graefes Arch. Clin. Exp. Ophthalmol.* **239**:109–113.
61. Picht, G., Welge-Luessen, U., Grehn, F., and Lutjen-Drecoll, E. 2001. Transforming growth factor beta 2 levels in the aqueous humor in different types of glaucoma and the relation to filtering bleb development. *Graefes Arch. Clin. Exp. Ophthalmol.* **239**:199–207.
62. Danielian, P.S., Muccino, D., Rowitch, D.H., Michael, S.K., and McMahon, A.P. 1998. Modification of gene activity in mouse embryos in utero by a tamoxifen-inducible form of Cre recombinase. *Curr. Biol.* **8**:1323–1326.
63. Soriano, P. 1999. Generalized lacZ expression with the ROSA26 Cre reporter strain. *Nat. Genet.* **21**:70–71.
64. Pankhurst, G.J., Bennett, C.A., and Easterbrook-Smith, S.B. 1998. Characterization of the heparin-binding properties of human clusterin. *Biochemistry.* **37**:4823–4830.
65. Kanegae, Y., et al. 1995. Efficient gene activation in mammalian cells by using recombinant adenovirus expressing site-specific Cre recombinase. *Nucleic Acids Res.* **23**:3816–3821.